

# Influence of Native Ureolytic Microbial Community on Biocementation Potential of *Sporosarcina Pasteurii*

**Raja Murugan**

Indian Institute of Technology Madras

**G. K. Suraishkumar**

Indian Institute of Technology Madras

**Abhijit Mukherjee**

Curtin University

**Navdeep K Dhami** (✉ [navdeep.dhami@curtin.edu.au](mailto:navdeep.dhami@curtin.edu.au))

Curtin University

---

## Research Article

**Keywords:** Native Ureolytic Microbial Community, Biocementation Potential, *Sporosarcina Pasteurii*

**Posted Date:** July 9th, 2021

**DOI:** <https://doi.org/10.21203/rs.3.rs-687770/v1>

**License:**  This work is licensed under a Creative Commons Attribution 4.0 International License.

[Read Full License](#)

---

# 1           **Influence of Native Ureolytic Microbial Community on** 2           **Biocementation Potential of *Sporosarcina pasteurii***

3           Raja Murugan<sup>1,2</sup>, G. K. Suraishkumar<sup>1</sup>, Abhijit Mukherjee<sup>2</sup>, Navdeep K Dhami<sup>2</sup>

4           <sup>1</sup>Bhupat and Jyoti Mehta School of Biosciences, Indian Institute of Technology Madras,  
5           Chennai – 600036, India.

6           <sup>2</sup>School of Civil and Mechanical Engineering, Curtin University, Western Australia – 6102,  
7           Australia.

8           Correspondence and requests for material should be addressed to N.K.D. (email:  
9           navdeep.dhami@curtin.edu.au)

## 10       **ABSTRACT**

11       Microbially induced calcium carbonate precipitation (MICP)/Biocementation has emerged as  
12       a promising technique for soil engineering applications. There are chiefly two methods by  
13       which MICP is applied for field applications including biostimulation and bioaugmentation.  
14       Although bioaugmentation strategy using efficient ureolytic biocementing culture of  
15       *Sporosarcina pasteurii* is widely practiced, the impact of native ureolytic microbial  
16       communities (NUMC) on CaCO<sub>3</sub> mineralisation via *S. pasteurii* has not been explored. In this  
17       paper, we investigated the effect of different concentrations of NUMC on MICP kinetics and  
18       biomineral properties in the presence and absence of *S. pasteurii*. Kinetic analysis showed that  
19       the biocementation potential of *S. pasteurii* is 6-fold higher than the NUMC and is not  
20       significantly impacted even when the concentration of the NUMC is eight times higher.  
21       Micrographic results revealed a quick rate of CaCO<sub>3</sub> precipitation by *S. pasteurii* led to the  
22       generation of smaller CaCO<sub>3</sub> crystals (5 - 40 μm), while the slow rate of CaCO<sub>3</sub> precipitation  
23       by NUMC led to the creation of larger CaCO<sub>3</sub> crystals (35 - 100 μm). Mineralogical results

24 showed the predominance of the calcite phase in both sets. The outcome of the current study is  
25 crucial for tailor-made applications of MICP.

## 26 INTRODUCTION

27 Microbially induced calcium carbonate precipitation (MICP) is a ubiquitously recorded process  
28 in nature and is responsible for the creation of numerous geological formations in terrestrial  
29 and marine environments<sup>1</sup>. Recently this process has been replicated in the lab conditions for  
30 numerous engineering applications, as it leads to the formation of carbonate cement at ambient  
31 temperature conditions by harnessing the cementation potential of living microorganisms. The  
32 major applications include improvement of mechanical properties of soil<sup>2,3</sup>, bioremediation of  
33 heavy metals and radio nucleotides<sup>4-6</sup>, enhancement of oil recovery<sup>7</sup>, repair of concrete  
34 cracks<sup>8,9</sup>, and sequestration of atmospheric CO<sub>2</sub><sup>10</sup>. The chief benefit of this bio-mimicked  
35 cementation process includes self-healing ability, eco-friendliness, recyclability, and low  
36 viscosity paving the way for deeper penetration<sup>11</sup>.

37 MICP/Biocementation occurs via various metabolic pathways of bacteria such as ureolysis,  
38 denitrification, sulfate reduction, and iron reduction<sup>12</sup>. Amongst the different pathways, MICP  
39 via ureolytic pathway is the most widely explored route because of its straightforwardness,  
40 efficacy, short time, and no excess production of protons<sup>13,14</sup>. In the microbial ureolytic  
41 pathway, urea is hydrolysed into ammonia and carbon dioxide by the action of urease<sup>2</sup>.  
42 Subsequently, these products equilibrate in water to form bicarbonate, ammonium, and  
43 hydroxide ions, which elevate the pH of the microenvironment around the bacteria (equation  
44 1). An increase in pH favors the equilibrium shifts from bicarbonate ions to carbonate ions.  
45 The formed carbonate ions then precipitate as calcium carbonate on the bacterial surface in the  
46 presence of calcium<sup>2</sup> (equation 2).



49 For applications of MICP in soils, especially in the field, there are two modes by which  
50 calcifying bacteria are supplemented: biostimulation (enrichment of native population) or  
51 bioaugmentation (supplementation of efficient foreign bacteria). The biostimulation approach  
52 deals with the modification of existing field conditions by altering the nutrients, substrates, and  
53 electron acceptors to enrich the native microorganisms for accelerating the  $\text{CaCO}_3$   
54 precipitation; whereas, bioaugmentation includes the addition of highly potential ureolytic and  
55 cementing strains especially *Sporosarcina pasteurii* into the fields<sup>32-36</sup>. Comparing these two  
56 approaches, MICP through bioaugmentation has a major advantage as it is a rapid process. This  
57 benefit makes this approach quite attractive for engineering applications, despite having the  
58 limitation of cost factor for preparation and transport of bacterial cultures<sup>35</sup>. On the other hand,  
59 biostimulation utilizes native bacteria making the MICP process both economically and  
60 environmentally viable<sup>35</sup>. Furthermore, the stimulation approach may eliminate the possible  
61 ecological impacts caused by a non-indigenous bacterial introduction in the applied soil  
62 environment, but the process rate is generally slow in comparison to the bioaugmentation  
63 approach<sup>37</sup>. The studies conducted on utilisation of both the approaches for improving the soil  
64 engineering properties reported that changes in solution chemistry and distribution of  $\text{CaCO}_3$   
65 precipitate occurred invariably in 1-meter soil column during biostimulation<sup>37</sup>; however,  
66 bioaugmentation with *S. pasteurii* led to significant improvement in strength, stiffness, load-  
67 bearing capacity and hydraulic conductivity of the soil<sup>12,37,38</sup>. Although researchers have  
68 demonstrated biogeochemical changes during the biostimulation approach, not much has been  
69 investigated on the impact of native ureolytic microbial communities (NUMC) on the  
70 performance of *S. pasteurii* and how these communities perform in comparison to this high  
71 urease producing culture<sup>37</sup>. Also, the concentration of NUMC changes vastly in the field and  
72 may affect the kinetics of the  $\text{CaCO}_3$  process, its mineralogy, and morphology which are the  
73 determining factors for the success of biocementation<sup>22</sup>.

74 Kinetic aspects of the CaCO<sub>3</sub> precipitation decide the overall efficacy of biocementation and  
75 are influenced by both abiotic and biotic factors including temperature, pH, aeration, nutrient  
76 availability, bacterial concentration, and type of bacteria or type of microbial population<sup>15-21</sup>.  
77 Amongst all these factors, the concentration of bacteria and urease enzyme is a crucial factor<sup>22</sup>  
78 and is reflected in the kinetic constant of the CaCO<sub>3</sub> precipitation in terms of first-order rate  
79 constant of 0.002 to 0.60 h<sup>-1</sup> <sup>23-25</sup>. Further, the kinetics of the process also control the  
80 morphological and nanomechanical properties of the precipitated CaCO<sub>3</sub>; the slow rate of  
81 precipitation leads to the production of larger-sized crystals that are relatively stable compared  
82 to the smaller crystals formed at a high rate of precipitation<sup>26,27</sup>.

83 In general, microbially induced CaCO<sub>3</sub> precipitate is a cohesive material<sup>2</sup> and exists in different  
84 crystalline phases including calcite, vaterite, aragonite, monohydrocalcite, and ikaite<sup>1</sup>. The  
85 sizes of these crystals vary from 5 – 100 μm along with variations in their nanomaterial  
86 properties <sup>28-30</sup>. Essential properties such as size, shape, stability, solubility, and hardness of  
87 the CaCO<sub>3</sub> crystals determine the efficacy of MICP in engineering applications. For example,  
88 the conservation of building materials required more stable calcite than metastable vaterite and  
89 larger rhombohedral crystals (100 – 150 μm) are more preferable in soil stabilization  
90 applications<sup>31</sup>. But very little information is available on these aspects including the impact of  
91 native communities on MICP kinetics with and without *S. pasteurii*, the effect of the  
92 concentration of native communities on MICP, and the influence of kinetic factors on morpho-  
93 mineralogical properties of carbonate crystals. All these factors are crucial in determining the  
94 efficacy of biocementation for field applications. The purpose of this study is to

95 1) evaluate the influence of native ureolytic microbial community (NUMC) at varying  
96 concentrations on biocementation kinetics 2) analyse the bioaugmentation potential of *S.*  
97 *pasteurii* in presence of different concentrations of native ureolytic microbial community and

98 3) investigate the effect of different cell concentrations of NUMC on morphological-  
99 mineralogical properties of *S. pasteurii* driven MICP.

100 We hypothesize that the outcome of this study will help to tailor MICP kinetics, morphology,  
101 mineralogy, and material properties of biomineralised crystals via both the stimulation and  
102 augmentation approach.

## 103 **RESULTS**

### 104 **Influence of the native ureolytic microbial community on the kinetics of calcium** 105 **carbonate precipitation**

106 To investigate the influence of native ureolytic microbial community (NUMC) on calcium  
107 carbonate precipitation at varying concentrations (0, 0.1, 0.2, 0.4, 0.8, 1.6, and 3.2 OD), soluble  
108 calcium concentration in the cementation medium was monitored for up to 288 hours (at an  
109 interval of 12 hours). From fig. 1a it can be observed that the soluble calcium concentration  
110 decreased over time in all the groups with varying rates except group A to which no NUMC  
111 was added. The calcium concentration decreased to 50% from the initial value for group B at  
112 96<sup>th</sup> hour, for group C at 60<sup>th</sup> hour, for group D at 48<sup>th</sup> hour, for group E at 36<sup>th</sup> hour, and group  
113 F and G at the 24<sup>th</sup> hour. At the end of the process, the soluble calcium ions in all the sets were  
114 exhausted, except in set A.

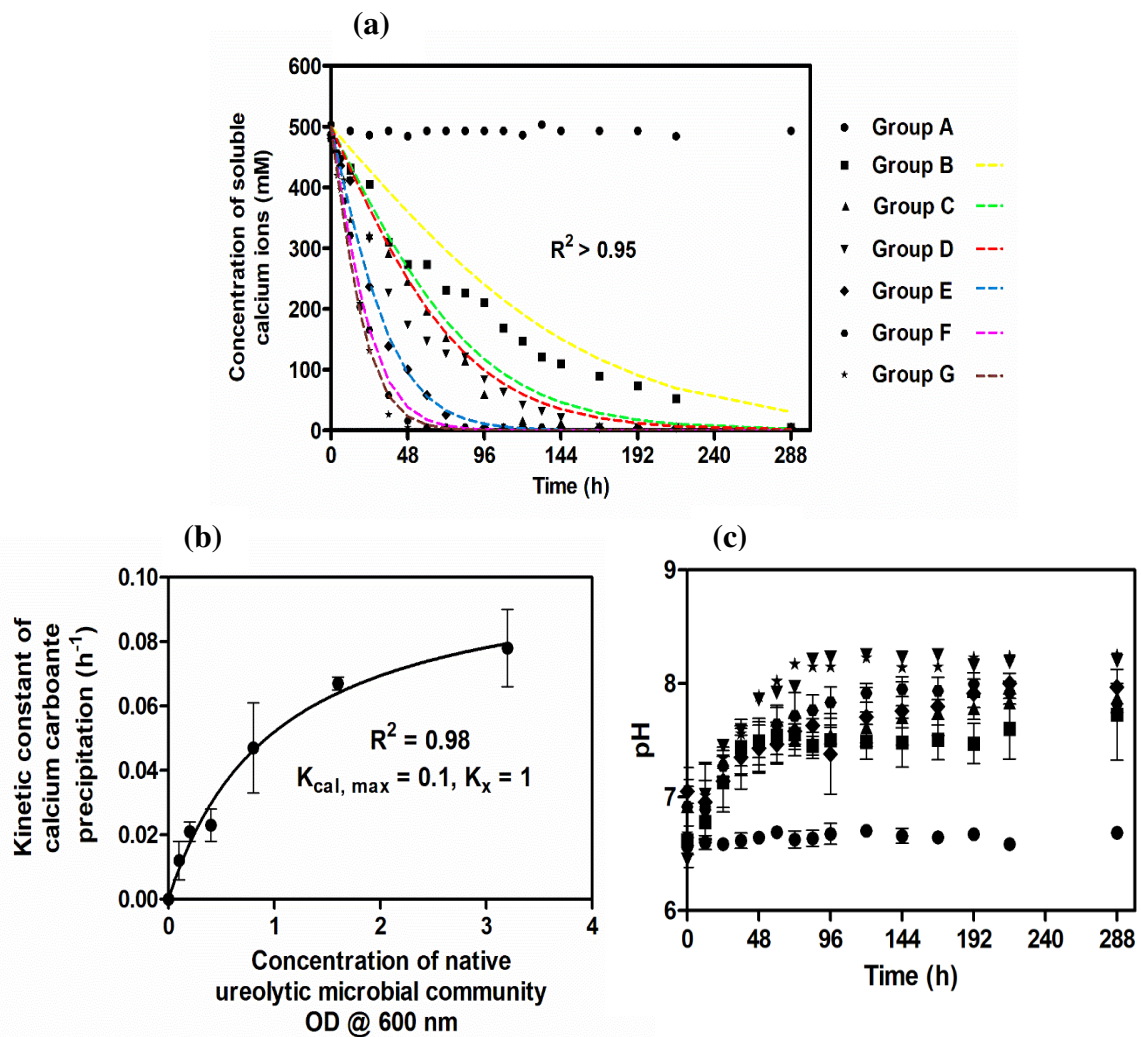
115 Kinetic constants ( $K_{\text{cal}}$ ) of  $\text{CaCO}_3$  precipitation were used to further investigate the effect of  
116 various parameters on carbonate precipitation<sup>36</sup>. The monitored profiles were computationally  
117 fitted using equation (4) to calculate  $K_{\text{cal}}$  values (Fig 1a). Table 1 shows  $K_{\text{cal}}$  values at varying  
118 NUMC. The  $K_{\text{cal}}$  values of the fitted graphs increased from group A ( $0 \text{ h}^{-1}$ ) to group G ( $0.078$   
119  $\text{h}^{-1}$ ). Further, it was found that the  $K_{\text{cal}}$  values can be described by a Michelis-Menten (MM)  
120 type equation (3) where  $K_x$  is a constant value,  $X$  is the bacterial concentration, and  $K_{\text{cal, max}}$  is  
121 the maximum kinetic constant for calcium carbonate precipitation. When  $K_x$  is equal to  $X$ , the

122 value of  $K_{cal}$  is equal to half of the  $K_{cal, max}$ . The observed values are  $K_x = 1$  OD and  $K_{cal, max} =$   
 123  $0.1 \text{ h}^{-1}$  in this study. Fig. 1b shows MM type plot that relates  $K_{cal}$  and NUMC concentration.

124 
$$K_{cal} = \frac{K_{cal,max} X}{K_x + X} \quad (3)$$

125 Fig. 1c shows the pH change over time in all the sets. In the cementation medium, pH was  
 126 observed to be between 6.5 and 8.3 in all the groups throughout the process. It can be seen that  
 127 the rate of pH change within the groups followed a similar trend except for the control group

128 A.



129 **Figure 1. Concentration of soluble calcium ions over time (a). The relationship between**  
 130 **the kinetic constant of  $\text{CaCO}_3$  precipitation and concentration of the native ureolytic**  
 131 **microbial community (b). The variation of pH with time (c). Group A – 0 OD NUMC,**  
 132 **Group B – 0.1 OD NUMC, Group C – 0.2 OD NUMC, Group D – 0.4 OD NUMC, Group E –**  
 133 **0.8 OD NUMC, Group F – 1.6 OD NUMC, and Group G – 3.2 OD NUMC. NUMC – Native**

134 Ureolytic Microbial Community. The coloured hidden lines are computationally fitted curves.  
 135 Error bars in the figure indicate the standard deviation of three independent trials.

S. No	Native ureolytic microbial community Group ID	Concentration of NUMC OD @ 600 nm	Kinetic constant Of calcium carbonate precipitation ( $\text{h}^{-1}$ )	$R^2$
1	Group A	0	0	NA
2	Group B	0.1	$0.012 \pm 0.006$	0.97
3	Group C	0.2	$0.021 \pm 0.003$	0.98
4	Group D	0.4	$0.023 \pm 0.005$	0.98
5	Group E	0.8	$0.047 \pm 0.014$	0.99
6	Group F	1.6	$0.067 \pm 0.002$	0.99
7	Group G	3.2	$0.078 \pm 0.012$	0.98

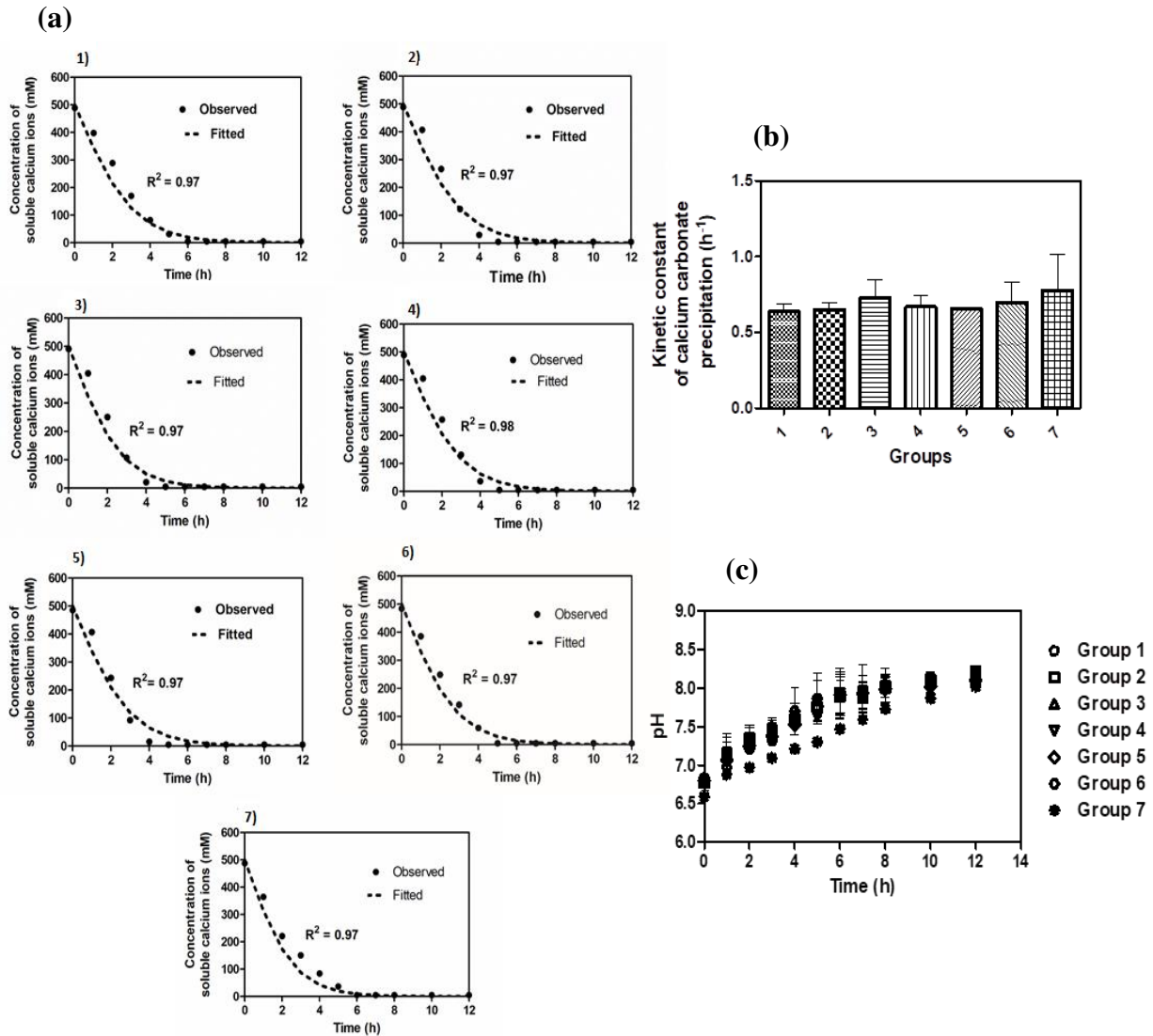
136 **Table 1. The kinetic constant values of  $\text{CaCO}_3$  precipitation at varying native ureolytic**  
 137 **microbial community concentration.** NUMC – Native Ureolytic Microbial Community. NA  
 138 – Not Applicable.  $\pm$  indicates the standard deviation of two independent trials.

139 **Influence of the native ureolytic microbial community on augmented *S. pasteurii***

140 To investigate the influence of NUMC on *S. pasteurii* (bioaugmentation), soluble calcium  
 141 concentration in the cementation medium was monitored over time and fitted with equation  
 142 (4). Fig. 2a shows both observed and fitted curves from groups 1 to 7. From this figure, an  
 143 exponential decrease of soluble calcium concentration was observed in all the groups with  
 144 immediate effect upon the addition of NUMC and *S. pasteurii*. The concentration was recorded  
 145 to be around zero at the 6<sup>th</sup> hour. From the fitted curves, the values of the kinetic constants for  
 146 calcium carbonate precipitation were calculated (Table 2) and compared (Fig. 2b). From Table  
 147 2 it can be seen that the kinetic constant values are 0.64, 0.65, 0.64, 0.73, 0.67, 0.66, 0.70, and  
 148  $0.78 \text{ h}^{-1}$  for the groups 1 to 7, respectively, i.e., the values were distributed between 0.64 and



149 0.78 h<sup>-1</sup>. The change in the pH values of the cementation medium was also monitored (Fig. 2c)  
 150 and the observed values were found to be between 6.5 and 8 for all the groups.



151 **Figure 2. Concentration of soluble calcium ions over time - Bioaugmentation (a),**  
 152 **comparison of the kinetic constant of CaCO<sub>3</sub> precipitation – Bioaugmentation (b), the**  
 153 **variation of pH with time (c). Group 1 - 0 OD NUMC + 0.4 OD *S. pasteurii*, Group 2 - 0.1**  
 154 **OD NUMC + 0.4 OD *S. pasteurii*, Group 3 - 0.2 OD NUMC + 0.4 OD *S. pasteurii*, 4) Group**  
 155 **4 - 0.4 OD NUMC + 0.4 OD *S. pasteurii*, 0.8 OD NUMC + 0.4 OD *S. pasteurii*, 1.6 OD NUMC**  
 156 **+ 0.4 OD *S. pasteurii*, and 3.2 OD NUMC + 0.4 OD *S. pasteurii*. NUMC – Native Ureolytic**  
 157 **Microbial Community. Bioaugmentation – (NUMC + *S. pasteurii*). Error bars in the figure 2b**  
 158 **and 2c indicate the standard deviation of two independent trials.**

S. No	Group ID	Concentration of NUMC OD @ 600 nm	Concentration of <i>S. pasteurii</i> OD@ 600 nm	Kinetic constant of CaCO <sub>3</sub> precipitation (h <sup>-1</sup> )	R <sup>2</sup>
1	Group 1	0		0.64 ± 0.05	0.97
2	Group 2	0.1		0.65 ± 0.05	0.97

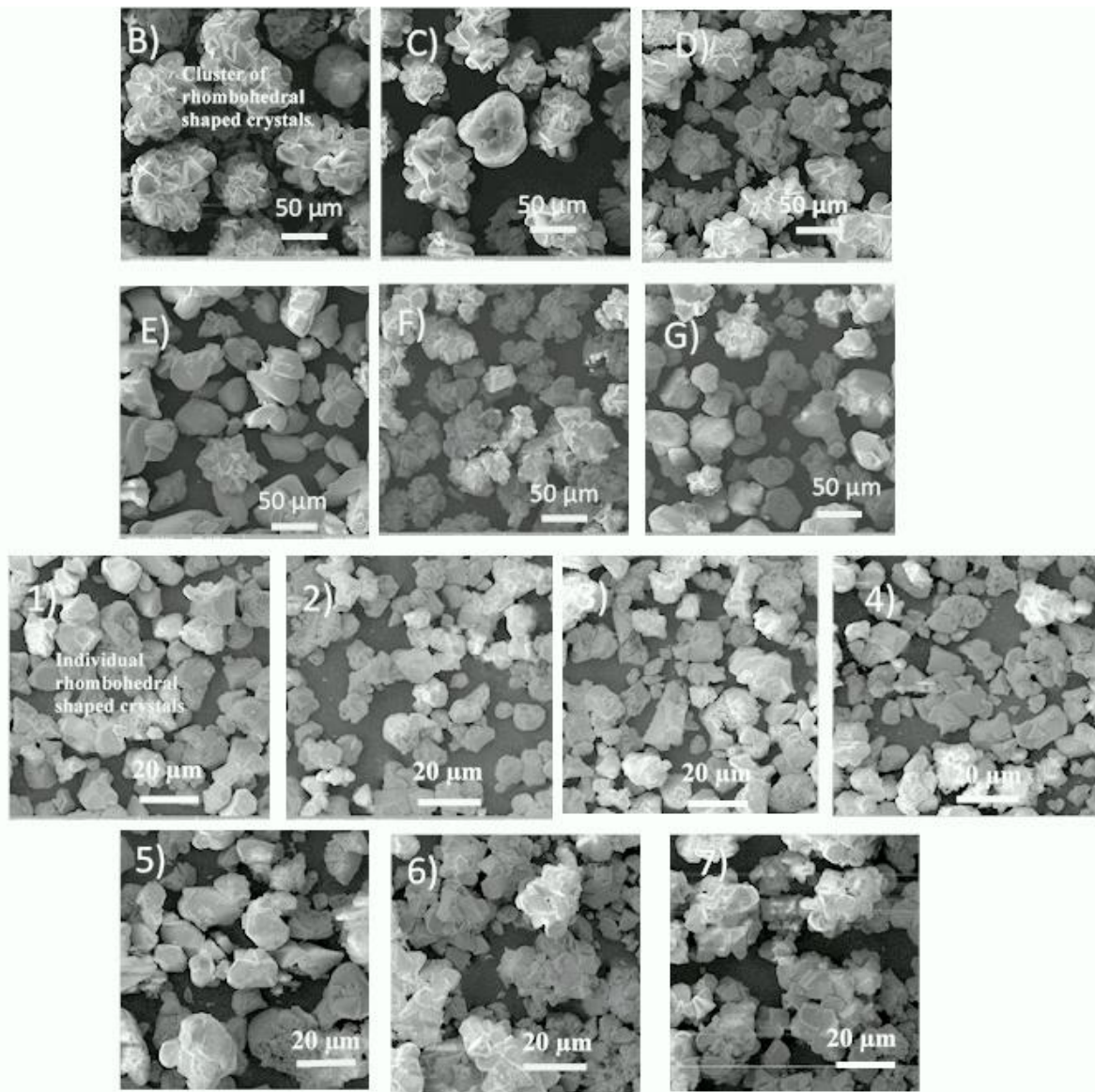
3	Group 3	0.2	0.4	$0.73 \pm 0.12$	0.97
4	Group 4	0.4		$0.67 \pm 0.07$	0.98
5	Group 5	0.8		$0.66 \pm 0.00$	0.97
6	Group 6	1.6		$0.70 \pm 0.13$	0.97
7	Group 7	3.2		$0.78 \pm 0.24$	0.97

159 **Table 2. The kinetic constants of calcium carbonate precipitation.**  $\pm$  indicates the standard  
160 deviation of two independent trials. NUMC – Native Ureolytic Microbial Community. *S.*  
161 *pasteurii* – *Sporosarcina pasteurii*.

### 162 **Morphology and Phase of CaCO<sub>3</sub>**

163 CaCO<sub>3</sub> crystal morphology varies depending on the surface properties of the bacterial cell wall  
164 composition especially extracellular polymeric substances and the solution chemistry of the  
165 medium<sup>26</sup>. Hence, the shape and size of precipitated crystals were analysed via scanning  
166 electron micrography (Fig. 3). For groups 1 to 4, rhombohedral-shaped crystals of size 5 – 10  
167  $\mu\text{m}$  were observed for the samples collected at the 12<sup>th</sup> hour. For group 5, the size of the  
168 individual and clustered rhombohedral-shaped crystals was found to be 15 – 25  $\mu\text{m}$  for the  
169 samples collected at the 12<sup>th</sup> hour. For groups 6 and 7, for the samples collected at the 12<sup>th</sup> hour  
170 the size of both the clustered rhombohedral-shaped crystals was 30 – 40  $\mu\text{m}$ . SEM images  
171 showed a cluster of rhombohedral-shaped crystals for the samples collected at 288<sup>th</sup> hour for  
172 the groups B to G. The size of these crystals varied between 35 – 100  $\mu\text{m}$ . The polymorph is  
173 a determining factor of strength and hardness of CaCO<sub>3</sub> in MICP. Therefore, the qualitative  
174 and quantitative information of the CaCO<sub>3</sub> crystals were obtained using the powdered XRD  
175 technique (for the groups B to G at 288<sup>th</sup> hour and the groups 1 to 7 at the 12<sup>th</sup> hour). Fig. 4  
176 shows the XRD spectrum of group B and the representative spectrums of all the other groups.  
177 Tables 3 and 4 show the morphology and phase analysis of native ureolytic microbial  
178 community and bioaugmentation studies. It was observed that only group B showed 2.3 % of  
179 the vaterite phase of CaCO<sub>3</sub> crystals and all observed crystal phases of all the groups were of  
180 the calcite phase.

181



182 **Figure 3. Scanning electron microscopy images of CaCO<sub>3</sub> crystals. Groups B to G**  
 183 **(NUMC) and 1 to 7 (Bioaugmentation).** B) – 0.1 OD NUMC, C) – 0.2 OD NUMC, D) – 0.4  
 184 OD NUMC, E) – 0.8 OD NUMC, F) – 1.6 OD NUMC, and G) – 3.2 OD. 1) - 0 OD NUMC +  
 185 0.4 OD *S. pasteurii*, 2) - 0.1 OD NUMC + 0.4 OD *S. pasteurii*, 3) - 0.2 OD NUMC + 0.4 OD  
 186 *S. pasteurii*, 4) Group 4 - 0.4 OD NUMC + 0.4 OD *S. pasteurii*, 5) 0.8 OD NUMC + 0.4 OD  
 187 *S. pasteurii*, 6) 1.6 OD NUMC + 0.4 OD *S. pasteurii*, and 7) 3.2 OD NUMC + 0.4 OD *S.*  
 188 *pasteurii*. NUMC – Native Ureolytic Microbial Community and Bioaugmentation – (NUMC  
 189 + *S. pasteurii*).

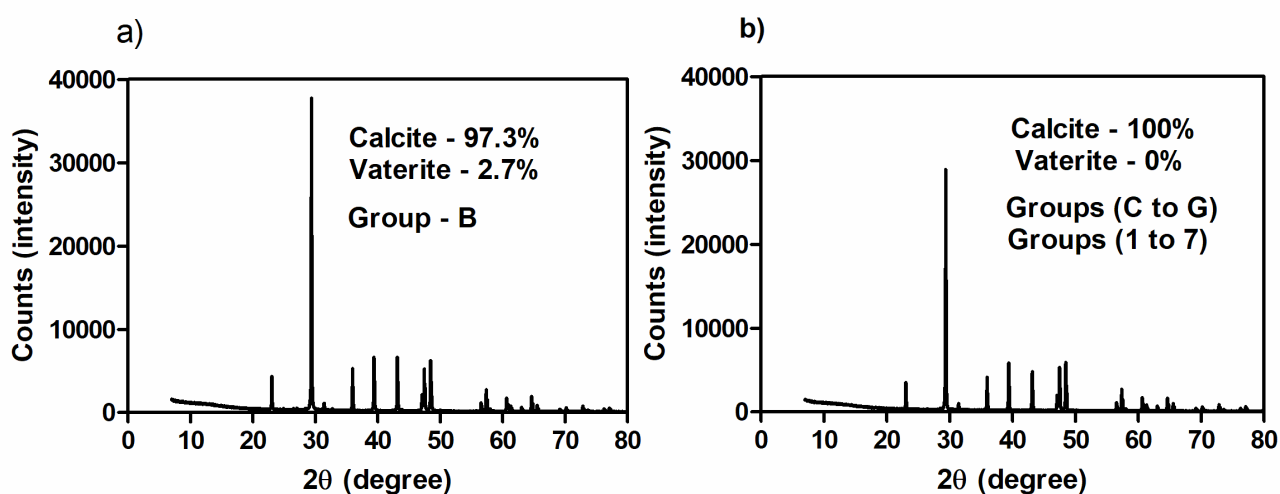
S. No	Group ID	Concentration of NUMC OD @ 600 nm	The average size of the crystal (µm)	Shape	Phase	
					Vaterite (%)	Calcite (%)
1	Group A	0	NA	NA	NA	NA
2	Group B	0.1	80 – 100	Cluster of rhombohedral	2.3	97.7
3	Group C	0.2	70 – 90	Cluster of rhombohedral	0	100
4	Group D	0.4	60 – 80	Cluster of rhombohedral	0	100

5	Group E	0.8	55 – 65	Individual and Cluster of rhombohedral	0	100
6	Group F	1.6	40 – 60	Individual and Cluster of rhombohedral	0	100
7	Group G	3.2	35 – 55	Individual and Cluster of rhombohedral	0	100

190 **Table 3. The influence of native ureolytic microbial community concentration on the**  
191 **morphology and phase of CaCO<sub>3</sub> crystals.** NUMC – Native Ureolytic Microbial Community.  
192 NA – Not Applicable.

S. No	Group ID	Concentration of NUMC OD @ 600 nm	Concentration of <i>S. pasteurii</i> OD@ 600 nm	The average size of the crystal (µm)	Shape	Phase
1	Group 1	0	0.4	5 – 10	Rhombohedral	Calcite
2	Group 2	0.1		5 – 10	Rhombohedral	
3	Group 3	0.2		5 – 10	Rhombohedral	
4	Group 4	0.4		5 – 10	Rhombohedral	
5	Group 5	0.8		15 – 25	Individual and cluster of rhombohedral	
6	Group 6	1.6		30 – 40	Cluster of rhombohedral	
7	Group 7	3.2		30 – 40	Cluster of rhombohedral	

193 **Table 4. The morphology and phase characterization of CaCO<sub>3</sub> crystals -**  
194 **Bioaugmentation.** NUMC – Native Ureolytic Microbial Community.



195 **Figure 4. XRD spectrum of CaCO<sub>3</sub> polymorphs. a) Group B (NUMC) and b) Groups C**  
196 **to G (NUMC) and 1 to 7 (bioaugmentation).** Group B – 0.1 OD NUMC, Group C – 0.2 OD  
197 NUMC, Group D – 0.4 OD NUMC, Group E – 0.8 OD NUMC, Group F – 1.6 OD NUMC,  
198 and Group G – 3.2 OD NUMC. Group 1 - 0 OD NUMC + 0.4 OD *S. pasteurii*, Group 2 - 0.1  
199 OD NUMC + 0.4 OD *S. pasteurii*, Group 3 - 0.2 OD NUMC + 0.4 OD *S. pasteurii*, 4) Group  
200 4 - 0.4 OD NUMC + 0.4 OD *S. pasteurii*, 0.8 OD NUMC + 0.4 OD *S. pasteurii*, 1.6 OD NUMC  
201 + 0.4 OD *S. pasteurii*, and 3.2 OD NUMC + 0.4 OD *S. pasteurii*. NUMC – Native Ureolytic  
202 Microbial Community, Bioaugmentation – (NUMC + *S. pasteurii*).

## 203 **DISCUSSION**

204 This study investigated the effect of NUMC on the augmented *S. pasteurii* by comparing the  
205 biocementing potentials of NUMC and augmented *S. pasteurii* in the presence of NUMC. To  
206 understand the effect, the kinetics of CaCO<sub>3</sub> precipitation, change in pH, the morphology of  
207 the CaCO<sub>3</sub> crystals formed and the phase of the precipitated crystals were analysed. The soluble  
208 calcium concentration was measured, and its kinetics was analysed using a logistic equation  
209 (4) to compare the biocementation potentials of NUMC and augmented *S. pasteurii* in the  
210 presence of NUMC. pH was also monitored to identify the range that favours CaCO<sub>3</sub>  
211 precipitation. SEM and XRD analyses were performed, which revealed the morphology (size  
212 and shape) and mineralogy of the crystals formed.

213 NUMC is capable of inducing CaCO<sub>3</sub> precipitation in their microenvironment<sup>39</sup>. In fig. 1a, the  
214 soluble calcium concentration decreased in all the groups. It could be due to carbonate ions  
215 generated in the MICP process during urea hydrolysis, which facilitates precipitation of soluble  
216 calcium around the bacterial cell wall in a cementation medium<sup>2</sup>. The complete exhaustion in  
217 the soluble calcium ions in the groups (group B – G) indicates that all the calcium in the  
218 medium is converted into CaCO<sub>3</sub>. Moreover, the supplied equimolar concentration of urea is  
219 enough for the complete conversion of CaCO<sub>3</sub>. The observed decrease in CaCO<sub>3</sub> precipitation  
220 rate (Fig. 1a) is due to encapsulation of CaCO<sub>3</sub> on the bacterial surface that limits the transport  
221 of nutrients transport including urea across the bacterial membrane<sup>40</sup>. The rate of soluble  
222 calcium depletion was observed to increase on increasing the NUMC concentration in the  
223 cementation medium. Increasing the NUMC concentration increases the total urease activity  
224 of the system, which in turn increases the soluble calcium depletion rate<sup>22</sup>. Moreover, the  
225 results show a positive correlation between CaCO<sub>3</sub> precipitation rate and the cell concentration  
226 <sup>22–24</sup>. Furthermore, the relationship between K<sub>cal</sub> and NUMC concentration could be used to  
227 design and develop a similar process for field applications. The kinetic constant K<sub>cal, Max</sub> in the

228 mathematical equation 3 denotes the maximum ability of the NUMC to achieve MICP at a  
229 faster rate, in this case,  $0.1 \text{ h}^{-1}$ . The kinetic constant  $K_x$  is equal to 1 OD, which indicates the  
230 concentration of NUMC required to achieve half the value of  $K_{\text{cal, Max}}$ .

231 *S. pasteurii* is a widely employed bacterial strain for bioaugmentation of soil consolidation and  
232 stabilization process because of its high urease-producing potential<sup>41</sup>. Hence, this bacterium  
233 was chosen as the model organism for this study. Supersaturation Index (SI) is one of the key  
234 parameters for the initiation of  $\text{CaCO}_3$  precipitation<sup>32</sup>. Quick  $\text{CaCO}_3$  precipitation was observed  
235 for groups 1-7 in the cementation medium. This indicates that the cementation medium has  
236 reached the required SI in a short time. pH also affects the SI, which is evident from the reported  
237 result<sup>42</sup> (Fig. 2c). Moreover, the ready availability of the positively charged calcium ions in the  
238 vicinity of the negatively charged bacterial surface could also favour quick  $\text{CaCO}_3$   
239 precipitation<sup>3</sup>.

240 The observed  $K_{\text{cal}}$  value of group 1 ( $0.64 \text{ h}^{-1}$ ) with *S. pasteurii* of 0.4 OD was 6-fold higher  
241 than the  $K_{\text{cal, Max}}$  ( $0.1 \text{ h}^{-1}$ ) value of NUMC. This indicates that *S. pasteurii* has relatively high  
242  $\text{CaCO}_3$  precipitation potential compared to NUMC. However, the observed results are in  
243 contrast to the reported studies that suggest biostimulation is the best possible approach for  
244 biocementation<sup>39,43</sup>. This could be due to the presence of different NUMC and varying study  
245 conditions between different research groups. The influence of varying concentrations of  
246 NUMC on the bioaugmentation potential of *S. pasteurii* was also investigated. However, no  
247 significant changes in the  $K_{\text{cal}}$  values were observed within the groups when  $K_{\text{cal}}$  values were  
248 compared between groups 1 to 7 (Fig. 2b). This indicates that the presence of NUMC did not  
249 influence the  $\text{CaCO}_3$  precipitation potential of *S. pasteurii* even at a concentration as high as  
250 8-fold (group 7) over a period of two weeks in this study.

251 The pH of the cementation medium greatly influences the  $\text{CaCO}_3$  precipitation and also affects  
252 bacterial urease production<sup>42</sup>. In this study, the pH of the cementation medium of all the groups

253 irrespective of the group type varied between 6.5 to 8.3. This indicates that the  $\text{CaCO}_3$   
254 precipitation occurred between the observed pH range. Urease activity of the bacteria results  
255 in the generation of ammonium ions that in turn affects the pH of the cementation medium.  
256 The rate of pH change was observed to be comparatively high for groups 1 to 7, which could  
257 be attributed to the high urease activity of *S. pasteurii*<sup>44</sup>. However, the same was not observed  
258 in groups A to G which could be attributed to the low urease activity of NUMC.

259 The molecular mechanism of  $\text{CaCO}_3$  crystal nucleation, growth, and morphology (size and  
260 shape) in the biocementation process is a complex phenomenon. Nature of the bacterial  
261 community, solution chemistry of the cementation medium (supersaturation index), the  
262 concentration of nutrients, calcium, and  $\text{Mg}^{2+}$  ions significantly influence the crystal growth  
263 kinetics and characteristics<sup>45,46,48</sup>. In this study, groups B to G with only NUMC at different  
264 concentrations showed a cluster of rhombohedral-shaped crystals, sized 35 -100  $\mu\text{m}$  at 288<sup>th</sup>  
265 hour. Whereas groups 1 to 4 with *S. pasteurii* in particular, yielded individual crystals of size  
266 5 - 10  $\mu\text{m}$  at 12<sup>th</sup> hour. A decrease in crystal size during bioaugmentation is due to the high  
267 driving force, which results in the fast attaining of the saturation state during  $\text{CaCO}_3$   
268 precipitation. According to the classical nucleation theory: the nucleus size of the crystal  
269 decreases when the driving force to reach the saturation state for the precipitation increases<sup>47</sup>.

270 This result is consistent with a previous study by Cuthbert and co-workers who reported that a  
271 higher initial saturation state influences the lower-sized crystals<sup>40</sup>.

272 The generation of ammonium ions and inorganic carbon due to the effective urea hydrolysis  
273 increases the pH and alkalinity of the cementation medium. It develops the oversaturated  
274 cementation solution that leads to the spontaneous  $\text{CaCO}_3$  precipitation<sup>32</sup>. It is possible to  
275 obtain different phases of  $\text{CaCO}_3$  including aragonite, calcite, vaterite, and two hydrated  
276 crystalline phases as monohydric calcite and ikaite in the MICP process<sup>1</sup>. This is because the  
277 polymorphism of  $\text{CaCO}_3$  is highly dependent on various parameters of the precipitation

278 environment. In general, many studies reported that the phase transition from metastable  
279 vaterite phase to more stable calcite phase during the  $\text{CaCO}_3$  precipitation process<sup>22,26</sup>. But, the  
280 specific phase preference by different bacterial cultures could depend on several parameters  
281 including the type of bacteria, specific amino acid sequences of urease, organic acid  
282 production, extracellular polymeric substances of the bacteria, the kinetics of the precipitation  
283 process, cementation medium composition, and other physicochemical parameters that affect  
284 supersaturation index of the solution<sup>48-52</sup>.

285 In this study, no visible  $\text{CaCO}_3$  crystals were observed in group A due to a lack of bacterial  
286 metabolic activity that leads to the undersaturation of the system. In the case of group B, besides  
287 97.7 % of calcite, 2.3 % of vaterite form of  $\text{CaCO}_3$  crystals were formed at the end 288<sup>th</sup> hour.  
288 On the other hand, in all other groups including group C to G and group 1 to 7 only calcite  
289 form of  $\text{CaCO}_3$  crystals was observed at the end of precipitation. From the results, it is evident  
290 that calcite is the predominant polymorph of  $\text{CaCO}_3$  crystals in both cases. It is also evident  
291 that the presence of NUMC does not affect calcite formation. Moreover, the observed results  
292 follow the Ostwald rule of crystallization, which states that thermodynamically crystal  
293 formation favors the less soluble calcite than more soluble vaterite<sup>27</sup>. There could be a possible  
294 delay in the transformation of vaterite to calcite form when the rate of  $\text{CaCO}_3$  precipitation is  
295 slow. Hence, this could be attributed to the slow transformation of vaterite to calcite in groups  
296 B to G<sup>27</sup>. Nevertheless, only rhombohedral-shaped calcite form of crystals was observed in all  
297 the groups despite different bacteria employed in this study at the end of the process. These  
298 calcite form crystals have superior engineering properties (strength and stiffness) compared to  
299 vaterite and aragonite forms of  $\text{CaCO}_3$  crystals.

### 300 **Conclusions**

301 In this study, we investigated the influence of native ureolytic microbial communities (NUMC)  
302 on the biocementation potential of the most widely used bacterial culture *Sporosarcina*



303 *pasteurii*. We evaluated the biogenic CaCO<sub>3</sub> precipitation kinetics of NUMC at varying  
304 concentrations in the presence and absence of *S. pasteurii* along with its impact on the morpho-  
305 mineralogical characteristics of the precipitated carbonates. Our key findings were that the  
306 concentration of cells has a major impact on the reaction kinetics as well as morpho-  
307 mineralogical properties of precipitated carbonate crystals as we recorded in the case of NUMC  
308 as well as *S. pasteurii*. The rate of ureolysis and calcium carbonate precipitation in the case of  
309 NUMC is very slow compared to *S. pasteurii*; and this can have a major impact on its  
310 application. *S. pasteurii* is highly efficient in biocementation even in the presence of native  
311 ureolytic cultures at different concentrations. Ureolytic and calcium carbonate precipitation  
312 kinetics of *S. pasteurii* were not found to be impacted significantly in the presence of NUMC;  
313 even when their concentration is eight folds higher. Although the rate of ureolysis and  
314 carbonate precipitation is low in the case of NUMC, but it has a positive impact on the quality  
315 of crystals. The size of calcite crystals in the case of NUMC with low metabolic activity is  
316 much higher (6-10 times) compared to smaller crystals formed by *S. pasteurii*. This  
317 demonstrates that depending upon the nature of application and time frame for cementation in  
318 field-scale/ other areas, it is crucial to have the fundamental information on biocementation  
319 potential of native communities and then look for alternatives as supplementation of *S.*  
320 *pasteurii*. Taken together, the results from the current study demonstrate, for the first time, that  
321 the quantitative and qualitative properties of biocement can be tailored utilising the information  
322 of ureolytic and carbonate precipitation kinetics with native as well as augmented cultures. This  
323 finding can enable several new possibilities for ureolysis driven biocementation in the area of  
324 advanced functional living materials.

## 325 **MATERIALS AND METHODS**

### 326 **Bacteria, Growth medium, and OD measurement**

327 The bacteria used in this study are the Native Ureolytic Microbial Community (NUMC)<sup>53</sup> and  
328 *S. pasteurii* (ATCC 11859). The bacteria were grown in Ammonium -Yeast extract medium  
329 (ATCC 1376) contains yeast extract (20 g/L), ammonium sulphate (10 g/L), and 0.13 M tris  
330 base (pH 9) were maintained at 30 °C and 180 rpm. The individual components of the growth  
331 medium were autoclaved and mixed after cooling under sterile conditions. To measure the  
332 concentration of the overnight grown NUMC and *S. pasteurii*, the media containing bacteria  
333 were centrifuged at 4500 rpm for 10 minutes and the optical density was measured using a  
334 spectrophotometer (Thermo scientific, Genesis 10S) at 600 nm with 0.85 % sodium chloride  
335 solution as blank.

### 336 **Cementation medium and conditions**

337 The cementation medium provides required nutrients and cementation components for NUMC  
338 and *S. pasteurii*. 100 mL of cementation medium was prepared by mixing 65 mL of autoclaved  
339 distilled water containing 0.2 g of yeast extract followed by the addition of required  
340 concentrations of NUMC and *S. pasteurii* cell pellet obtained after centrifugation (4500 rpm  
341 for 10 minutes). Then 10 and 25 mL of filter-sterilized 5 M urea and 2 M calcium chloride  
342 dihydrate solution were added, respectively. The cementation medium containing a bacterial  
343 pellet was maintained at 30 °C and 180 rpm in a shaker incubator.

### 344 **Enumeration of bacterial concentration**

345 The bacterial concentration was measured by the serial dilution method. Petri plates containing  
346 1.5 % agar in ATCC 1376 media were used to spread the bacteria; 1 OD of bacteria in saline  
347 was found to contain cells equivalent to  $4.5 \times 10^8$  cells/mL.

## 348 **Study design**

349 This study was designed to investigate the influence of NUMC on the biocementation potential  
350 of augmented *S. pasteurii*. The study was divided into two major groups. Each group is further  
351 subdivided into seven subgroups namely A to G and 1 to 7. The groups A, B, C, D, E, F, and  
352 G have overnight grown NUMC pellet mixed with cementation medium at concentrations of  
353 0, 0.1, 0.2, 0.4, 0.8, 1.6, and 3.2 OD, respectively. The groups 1, 2, 3, 4, 5, 6, and 7 contain  
354 fixed concentration of *S. pasteurii* (0.4 OD) and NUMC at concentrations of 0, 0.1, 0.2, 0.4,  
355 0.8, 1.6, and 3.2 OD, respectively in the cementation medium. To monitor the process, 2 mL  
356 of samples were taken and centrifuged at 3000 rpm for 10 minutes at regular intervals of time.  
357 The obtained supernatant was used to measure soluble calcium concentration and pH until the  
358 process was complete.

## 359 **Measurement of soluble calcium ions and pH**

360 The soluble calcium ions were measured by using the complexometric titration procedure<sup>54</sup>. 40  
361  $\mu\text{L}$  of the sample was diluted to 10 mL followed by the addition of 400  $\mu\text{L}$  1 N sodium  
362 hydroxide solution and a few drops of hydroxy naphthol blue disodium salt (1% W/V) solution  
363 indicators. Then the mixture was titrated against 1 mM EDTA disodium salt solution until the  
364 colour change from pink to blue was observed. The slope of the standard (0 – 2.5 mM  $\text{CaCl}_2$ )  
365 was used to calculate the actual concentration of calcium ions in the sample. The change in pH  
366 during biocementation was recorded using a pH meter (Thermo scientific, Orion star, A211).

## 367 **Morphology and phase analysis of $\text{CaCO}_3$**

368 The  $\text{CaCO}_3$  precipitate from the cementation medium was analysed at the end of the process.  
369 30 mL of sample was taken was centrifuged at 4500 rpm for 10 minutes. The pellets obtained  
370 were washed twice with distilled water and dried at 37 °C overnight. Then the dried crystals  
371 were subjected to scanning electron microscopy and XRD.

372 **Morphology (Size and Shape)**

373 The variable pressure electron microscope (VP – SEM, Zeiss, EVO 40 -XVP, 2008) was used  
374 to observe the size and shape of the CaCO<sub>3</sub> precipitate. The samples were placed on carbon-  
375 aluminum tape and coated using a carbon evaporative coater (creissington, 2080C, 2011). The  
376 beam intensity and voltage were 8.0 and 10 kV, respectively with a working distance of around  
377 15 mm. The secondary electron imaging was used to obtain scanning electron micrographs.  
378 The sizes of the crystals from the micrographs were obtained using IMAJEJ (1.8.0 172)  
379 software.

380 **Phase**

381 Bruker D8 advance diffractometer with Ni-filtered Cu K $\alpha$  radiation (40 kV, 40 mA) over the  
382 range 7 – 120° 2 $\theta$ , with a step size of 0.015° was used to collect the XRD data. The powdered  
383 CaCO<sub>3</sub> was resuspended in ethanol and deposited onto low-background holders. Further, the  
384 phase identification was done in Bruker EVA 5.2 using the Crystallography Open Database  
385 (COD) (<http://www.crystallogrphy.net/>). The phase quantification was done in Topas  
386 Academic 7 using the Rietveld method. Also, the crystal structures were identified from the  
387 COD.

388 **Calculation of kinetic constants for calcium carbonate precipitation**

389 In this study, the soluble calcium concentration over time was fitted with equation 4 using the  
390 solver function in Excel (2016 MSO) to calculate kinetic constants of CaCO<sub>3</sub> precipitation.

391 
$$C_{cal}(t) = 2C_0 / (1 + e^{K_{cal} t}) \quad (4)$$

392 Where, C<sub>0</sub> = initial concentration of calcium (mM),

393 C<sub>cal</sub>(t) = soluble calcium concentration (mM) at given time,

394 t = time (h) and,

395 K<sub>cal</sub> = kinetic constant of calcium carbonate precipitation (h<sup>-1</sup>).

396 **References**

- 397 1. Dhami, N. K., Reddy, M. S. & Mukherjee, M. S. Biomineralization of calcium  
398 carbonates and their engineered applications: A review. *Front. Microbiol.* **4**, 1–14 (2013).
- 399 2. Stocks-Fischer, S., Galinat, J. K. & Bang, S. S. Microbiological precipitation of CaCO  
400 3. *Soil Biol. Biochem.* **31**, 1563–1571 (1999).
- 401 3. Dejong, J. T., Mortensen, B. M., Martinez, B. C. & Nelson, D. C. Bio-mediated soil  
402 improvement. *Ecol. Eng.* **36**, 197–210 (2010).
- 403 4. Ferris, F. G., Phoenix, V., Fujita, Y. & Smith, R. W. Kinetics of calcite precipitation  
404 induced by ureolytic bacteria at 10 to 20°C in artificial groundwater. *Geochim. Cosmochim.*  
405 *Acta* **68**, 1701–1710 (2004).
- 406 5. Fujita, Y., Grant Ferris, F., Daniel Lawson, R., Colwell, F. S. & Smith, R. W. Calcium  
407 carbonate precipitation by ureolytic subsurface bacteria. *Geomicrobiol. J.* **17**, 305–318  
408 (2000)
- 409 6. Kumari, D., Qian, X. Y., Pan, X., Achal, V. & Li, Q. Microbially-induced Carbonate  
410 Precipitation for Immobilization of Toxic Metals. *Adv. Appl. Microbiol.* **94**, 79–108 (2016).
- 411 7. Wu, J., Wang, X. B., Wang, H. F. & Zeng, R. J. Microbially induced calcium carbonate  
412 precipitation driven by ureolysis to enhance oil recovery. *RSC Adv.* **7**, 37382–37391 (2017).
- 413 8. Ramachandran, S. K., Ramakrishnan, V. & Bang, S. S. Remediation of concrete using  
414 micro-organisms. *ACI Mater. J.* **98**, 3–9 (2001).
- 415 9. Van Tittelboom, K., De Belie, N., De Muynck, W. & Verstraete, W. Use of bacteria to  
416 repair cracks in concrete. *Cem. Concr. Res.* **40**, 157–166 (2010).
- 417 10. Mitchell, A. C., Dideriksen, K., Spangler, L. H., Cunningham, A. B. & Gerlach, R.  
418 Microbially enhanced carbon capture and storage by mineral-trapping and solubility-  
419 trapping. *Environ. Sci. Technol.* **44**, 5270–5276 (2010).
- 420 11. Phillips, A. J. *et al.* Engineered applications of ureolytic biomineralization: A review.

- 421 *Biofouling* **29**, 715–733 (2013).
- 422 12. Van Paassen, L. A., Ghose, R., van der Linden, T. J. M., van der Star, W. R. L. & van  
423 Loosdrecht, M. C. M. Quantifying Biomediated Ground Improvement by Ureolysis: Large-  
424 Scale Biogrout Experiment. *J. Geotech. Geoenvironmental Eng.* **136**, 1721–1728 (2010).
- 425 13. Whiffin, V. S., van Paassen, L. A. & Harkes, M. P. Microbial Carbonate Precipitation  
426 as a Soil Improvement Technique. *Geomicrobiol. J.* **24**, 417–423 (2007).
- 427 14. Zhang, J. L. *et al.* Screening of bacteria for self-healing of concrete cracks and  
428 optimization of the microbial calcium precipitation process. *Appl. Microbiol. Biotechnol.*  
429 **100**, 6661–6670 (2016).
- 430 15. Mortensen, B. M., Haber, M. J., DeJong, J. T., Caslake, L. F. & Nelson, D. C. Effects  
431 of environmental factors on microbial induced calcium carbonate precipitation. *J. Appl.*  
432 *Microbiol.* **111**, 338–349 (2011).
- 433 16. Martinez, B. C. *et al.* Experimental Optimization of Microbial-Induced Carbonate  
434 Precipitation for Soil Improvement. *J. Geotech. Geoenvironmental Eng.* **139**, 587-598  
435 (2013).
- 436 17. Soon, N.W., Lee, L.M., Khun, T.C. & Ling, H.S. Factors Affecting Improvement in  
437 Engineering Properties of Residual Soil through Microbial-Induced Calcite Precipitation.  
438 *Artic. J. Geotech. Geoenvironmental Eng.* **140**, 04014006 (2014).
- 439 18. Zhao, Q. *et al.* Factors Affecting Improvement of Engineering Properties of MICP-  
440 Treated Soil Catalyzed by Bacteria and Urease. *J. Mater. Civ. Eng.* **26**, 04014094 (2014).
- 441 19. Oral, Ç. M. & Ercan, B. Influence of pH on morphology, size and polymorph of room  
442 temperature synthesized calcium carbonate particles. *Powder Technol.* **339**, 781–788  
443 (2018).
- 444 20. Li, M., Wen, K., Li, Y. & Zhu, L. Impact of Oxygen Availability on Microbially  
445 Induced Calcite Precipitation (MICP) Treatment. *Geomicrobiol. J.* **35**, 15–22 (2018).

- 446 21. Peng, J. & Liu, Z. Influence of temperature on microbially induced calcium carbonate  
447 precipitation for soil treatment. *PLoS One* **14**, e0218396 (2019).
- 448 22. Wen, K., Li, Y., Amini, F. & Li, L. Impact of bacteria and urease concentration on  
449 precipitation kinetics and crystal morphology of calcium carbonate. *Acta Geotech.* **15**, 17–  
450 27 (2020).
- 451 23. Okwadha, G. D. O. & Li, J. Optimum conditions for microbial carbonate precipitation.  
452 *Chemosphere* **81**, 1143–1148 (2010).
- 453 24. Lauchnor, E. G., Topp, D. M., Parker, A. E. & Gerlach, R. Whole cell kinetics of  
454 ureolysis by *Sporosarcina pasteurii*. *J. Appl. Microbiol.* **118**, 1321–1332 (2015).
- 455 25. Mitchell, A. C. *et al.* Kinetics of calcite precipitation by ureolytic bacteria under aerobic  
456 and anaerobic conditions. *Biogeosciences* **16**, 2147–2161 (2019).
- 457 26. Heveran, C. M. *et al.* Engineered Ureolytic Microorganisms Can Tailor the  
458 Morphology and Nanomechanical Properties of Microbial-Precipitated Calcium  
459 Carbonate. *Sci. Rep.* **9**, 1–13 (2019).
- 460 27. Mitchell, A. C. & Grant Ferris, F. The influence of *Bacillus pasteurii* on the nucleation  
461 and growth of calcium carbonate. *Geomicrobiol. J.* **23**, 213–226 (2006).
- 462 28. Hammes, F., Boon, N., De Villiers, J., Verstraete, W. & Siciliano, S. D. Strain-specific  
463 ureolytic microbial calcium carbonate precipitation. *Appl. Environ. Microbiol.* **69**, 4901–  
464 4909 (2003).
- 465 29. Rodriguez-Navarro, C., Jimenez-Lopez, C., Rodriguez-Navarro, A., Gonzalez-Muñoz,  
466 M. T. & Rodriguez-Gallego, M. Bacterially mediated mineralization of vaterite. *Geochim.*  
467 *Cosmochim. Acta* **71**, 1197–1213 (2007).
- 468 30. Chen, L. *et al.* Bacteria-mediated synthesis of metal carbonate minerals with unusual  
469 morphologies and structures. *Cryst. Growth Des.* **9**, 743–754 (2009).
- 470 31. Dhami, N. K., Mukherjee, A. & Reddy, M. S. Micrographical, mineralogical and nano-

471 mechanical characterisation of microbial carbonates from urease and carbonic anhydrase  
472 producing bacteria. **94**, 443–454 (2016).

473 32. Fujita, Y., Grant Ferris, F., Daniel Lawson, R., Colwell, F. S. & Smith, R. W. Calcium  
474 carbonate precipitation by ureolytic subsurface bacteria. *Geomicrobiol. J.* **17**, 305–318  
475 (2000).

476 33. Burbank, M. B., Weaver, T. J., Green, T. L., Williams, B. & Crawford, R. L.  
477 Precipitation of calcite by indigenous microorganisms to strengthen liquefiable soils.  
478 *Geomicrobiol. J.* **28**, 301–312 (2011).

479 34. Gomez, M. G. *et al.* Field-scale bio-cementation tests to improve sands. *Proc. Inst. Civ.*  
480 *Eng. Gr. Improv.* **168**, 206–216 (2015).

481 35. Gomez, M. G. *et al.* Large-Scale Comparison of Bioaugmentation and Biostimulation  
482 Approaches for Biocementation of Sands. *J. Geotech. Geoenvironmental Eng.* **143**,  
483 04016124 (2017).

484 36. Tobler, D. J. *et al.* Comparison of rates of ureolysis between *Sporosarcina pasteurii* and  
485 an indigenous groundwater community under conditions required to precipitate large  
486 volumes of calcite. *Geochim. Cosmochim. Acta* **75**, 3290–3301 (2011).

487 37. Gomez, M. G., Graddy, C. M. R., Dejong, J. T. & Nelson, D. C. Biogeochemical  
488 Changes During Bio-cementation Mediated by Stimulated and Augmented Ureolytic  
489 Microorganisms. *Sci. Rep.* 1–15 (2019).

490 38. Dhama, N. K., Alsubhi, W. R., Watkin, E. & Mukherjee, A. Bacterial community  
491 dynamics and biocement formation during stimulation and augmentation: Implications for  
492 soil consolidation. *Front. Microbiol.* **8**, 1267 (2017).

493 39. Raveh-Amit, H. & Tsesarsky, M. Biostimulation in desert soils for microbial-induced  
494 calcite precipitation. *Appl. Sci.* **10**, 2905 (2020).

495 40. Cuthbert, M. O. *et al.* Controls on the rate of ureolysis and the morphology of carbonate



496 precipitated by *S. Pasteurii* biofilms and limits due to bacterial encapsulation. *Ecol. Eng.*  
497 **41**, 32–40 (2012).

498 41. Gomez, M. G., DeJong, J. T., Anderson, C. M., Nelson, D. C. & Graddy, C. M. Large-  
499 Scale Bio-Cementation Improvement of Sands. in *Geotechnical and Structural*  
500 *Engineering Congress 2016 - Proceedings of the Joint Geotechnical and Structural*  
501 *Engineering Congress 2016* 941–949 (American Society of Civil Engineers, 2016).

502 42. Hammes, F. & Verstraete, W. Key roles of pH and calcium metabolism in microbial  
503 carbonate precipitation. *Rev. Environ. Sci. Biotechnol.* (2002).

504 43. Gomez, M. G., Graddy, C. M. R., DeJong, J. T., Nelson, D. C. & Tsesarsky, M.  
505 Stimulation of Native Microorganisms for Biocementation in Samples Recovered from  
506 Field-Scale Treatment Depths. *J. Geotech. Geoenvironmental Eng.* **144**, 04017098 (2018).

507 44. Bachmeier, K. L., Williams, A. E., Warmington, J. R. & Bang, S. S. Urease activity in  
508 microbiologically-induced calcite precipitation. *J. Biotechnol.* **93**, 171–181 (2002).

509 45. Okyay, T. O. & Rodrigues, D. F. Optimized carbonate micro-particle production by  
510 *Sporosarcina pasteurii* using response surface methodology. *Ecol. Eng.* **62**, 168–174  
511 (2014).

512 46. Chekroun, K. Ben *et al.* Precipitation and growth morphology of calcium carbonate  
513 induced by *Myxococcus xanthus*: Implications for recognition of bacterial carbonates. *J.*  
514 *Sediment. Res.* **74**, 868–876 (2004).

515 47. Oxtoby, D. W. Homogeneous nucleation: Theory and experiment. *J. Phys. Condens.*  
516 *Matter* **4**, 7627–7650 (1992).

517 48. Al Imran, M., Shinmura, M., Nakashima, K. & Kawasaki, S. Effects of Various Factors  
518 on Carbonate Particle Growth Using Ureolytic Bacteria. *Mater. Trans.* **59**, 1520–1527  
519 (2018).

520 49. Lee, Y. S. & Park, W. Current challenges and future directions for bacterial self-healing

521 concrete. *Appl. Microbiol. Biotechnol.* **102**, 3059–3070 (2018).

522 50. Sondi, I. & Salopek-Sondi, B. Influence of the primary structure of enzymes on the  
523 formation of CaCO<sub>3</sub> polymorphs: A comparison of plant (*Canavalia ensiformis*) and  
524 bacterial (*Bacillus pasteurii*) ureases. *Langmuir* **21**, 8876–8882 (2005).

525 51. Rodriguez-Blanco, J. D., Shaw, S. & Benning, L. G. The kinetics and mechanisms of  
526 amorphous calcium carbonate (ACC) crystallization to calcite, via vaterite. *Nanoscale* **3**,  
527 265–271 (2011).

528 52. Rodriguez-Navarro, C., Jroundi, F., Schiro, M., Ruiz-Agudo, E. & González-Muñoz,  
529 M. T. Influence of substrate mineralogy on bacterial mineralization of calcium carbonate:  
530 Implications for stone conservation. *Appl. Environ. Microbiol.* **78**, 4017–4029 (2012).

531 53. Dubey, A. et al. Biocementation mediated by stimulated ureolytic microbes from  
532 brahmaputra riverbank for mitigation of soil erosion. 26 February 2021, preprint (version  
533 1) available at research square [<https://doi.org/10.21203/rs.3.rs-235959/v1>].

534 54. APHA/AWWA/WEF. Standard Methods for the Examination of Water and  
535 Wastewater. *Stand. Methods* 541 (2012).

## 536 **Acknowledgments**

537 The authors would like to acknowledge the Microscopy and Microanalysis Facility, Curtin  
538 University, Western Australia for SEM and XRD analysis. The current study was funded by  
539 the Australian Research Council Linkage Project LP180100132.

## 540 **Authors Contributions**

541 R.M. performed the experiments; R.M., N.K.D., G.K.S., and A.M. contributed to experimental  
542 design and data analysis; R.M., and N.K.D. wrote the manuscript. All the authors reviewed the  
543 manuscript.

## 544 **Additional Information**

545 **Competing financial interests:** The authors declare no competing financial interests.